Accepted Manuscript

STAT1 as a downstream mediator of ERK signaling contributes to bone cancer pain by regulating MHC II expression in spinal microglia

Zhenpeng Song, Bingrui Xiong, Hua Zheng, Anne Manyande, Xuehai Guan, Fei Cao, Lifang Ren, Yaqun Zhou, Dawei Ye, Yuke Tian

PII: S0889-1591(16)30472-X
DOI: http://dx.doi.org/10.1016/j.bbi.2016.10.009
Reference: YBRBI 2988

To appear in: *Brain, Behavior, and Immunity*

Received Date: 14 June 2016
Revised Date: 8 October 2016
Accepted Date: 10 October 2016

Please cite this article as: Song, Z., Xiong, B., Zheng, H., Manyande, A., Guan, X., Cao, F., Ren, L., Zhou, Y., Ye, D., Tian, Y., STAT1 as a downstream mediator of ERK signaling contributes to bone cancer pain by regulating MHC II expression in spinal microglia, *Brain, Behavior, and Immunity* (2016), doi: http://dx.doi.org/10.1016/j.bbi.2016.10.009

STAT1 as a downstream mediator of ERK signaling contributes to bone cancer pain by regulating MHC II expression in spinal microglia

Zhenpeng Song[1,2 #], Bingrui Xiong[1 #], Hua Zheng[1], Anne Manyande[4], Xuehai Guan[5], Fei Cao[1], Lifang Ren[1], Yaqun Zhou[1], Dawei Ye[3 *], Yuke Tian[1 *]

[1]Department of Anesthesiology and Pain Medicine, Tongji Hospital, Tongji Medical College, Huazhong University of Science and Technology, Wuhan 430030, China; [2]Department of Pain Medicine, Binzhou Medical University Hospital, Binzhou 256600, China; [3]Cancer Center, Tongji Hospital, Tongji Medical College, Huazhong University of Science and Technology, Wuhan 430030, China; [4]School of Human and Social Sciences, University of West London, Middlesex TW8 9GA, UK; [5]Department of Anesthesiology, the People's Hospital of Guangxi Zhuang Autonomous Region, Nanning 530021, China

[*] Correspondence and request for materials should be addressed to Dawei Ye (dy0711@gmail.com) or Yuke Tian (yktian@tjh.tjmu.edu.cn). [#] Zhenpeng Song and Bingrui Xiong contributed equally to this work.

Abstract

Major histocompatibility class II (MHC II)-specific activation of $CD4^+$ T helper cells generates specific and persistent adaptive immunity against tumors. Emerging evidence demonstrates that MHC II is also involved in basic pain perception; however, little is known regarding its role in the development of cancer-induced bone pain (CIBP). In this study, we demonstrate that MHC II expression was markedly induced on the spinal microglia of CIBP rats in response to STAT1 phosphorylation. Mechanical allodynia was ameliorated by either pharmacological or genetic inhibition of MHC II upregulation, which was also attenuated by the inhibition of pSTAT1 and pERK but was deteriorated by intrathecal injection of IFNγ. Furthermore, inhibition of ERK signaling decreased the phosphorylation of STAT1, as well as the production of MHC II *in vivo* and *in vitro*. These findings suggest that STAT1 contributes to bone cancer pain as a downstream mediator of ERK signaling by regulating MHC II expression in spinal microglia.

Keywords: bone cancer pain; microglia; major histocompatibility complex class II; ERK; STAT1

Introduction

In 2016, 1,685,210 new cancer cases and an estimated 595,690 cancer deaths are projected to occur in the United States(Siegel et al., 2016). Malignant tumors such as those in lung, prostate, and breast can undergo skeletal metastases that could result in severe cancer-induced bone pain, which substantially reduces the quality of life in cancer patients(Selvaraj et al., 2015). Unfortunately, current treatments for bone cancer pain (BCP) are insufficient due to a lack of understanding of the underlying mechanisms.

Growing evidence suggests that the neuroimmune response plays a pivotal role in the development and maintenance of chronic pain(Dominguez et al., 2008; Grace et al., 2011; Sato-Takeda et al., 2006; Sweitzer and DeLeo, 2002); however, the precise mechanism is still largely unknown. Microglia are the resident macrophages of the central nervous system (CNS), which continuously survey the microenvironment. Any alteration of neuronal activity can induce specific microglial changes(Nimmerjahn et al., 2005). Under chronic pain or neuroinflammatory conditions, microglial cells are activated and express high levels of major histocompatibility complex class II (MHC II). The most recognized function of MHC II is to be constitutively expressed on the surface of professional antigen-presenting cells loaded with antigenic peptide(Roche and Furuta, 2015). Notably, many studies on the effects of spinal dorsal microglia suggest that MHC II may be a critical molecule in chronic neuropathic pain and autoimmune diseases(Hashizume et al., 2000; Lincoln et al., 2005; Sato-Takeda et al., 2006; Sweitzer et al., 2002). Therefore, modulating the expression of MHC II in spinal microglia to inhibit maladaptive neuroimmune responses could be a potential therapeutic strategy for pain relief.

The Janus kinase/signal transducer and activator of transcription 1 (JAK/STAT1) signaling pathway is a key regulator of MHC II expression by modulating the expression of class II transactivator (CIITA)(Nikodemova et al., 2007; Ting and Trowsdale, 2002). In particular, JAK/STAT1 signaling is not only activated by interferon γ (IFNγ)(Herrera-Molina et al., 2012; Muhlethaler-Mottet et al., 1998; Nikodemova et al., 2007; Zhou et al., 2015) but is also among the five pathways that lead to microglial activation(Graeber, 2010; Hanisch and Kettenmann, 2007; Smith, 2010). To date, no direct evidence links the JAK/STAT1 signaling pathway to tactile allodynia under BCP conditions. We recently reported that ERK signaling is involved in the pathogenesis of BCP(Guan et al., 2015a); moreover, the fact that the activation of ERK signaling potentiates STAT1 phosphorylation was reported by others(Herrera-Molina et al., 2012). In the present study, we investigated the role of MHC II in BCP. In particular, we analyzed the relationship between ERK and STAT1 in regulating MHC II expression *in vivo* in a BCP rat model and *in vitro* using primary microglial cultures.

Materials and Methods

Animals

Adult virgin female Sprague Dawley (SD) rats (weighing 200-220 g) used in the present study were purchased from the Experimental Animal Research Center of Hubei Province, Wuhan, China (No. 42000600003611). Twenty-four-hour-old rat pups were used for the preparation of primary microglia. All rats were kept under specific pathogen-free and climate-controlled conditions (temperature 23±1°C, relative humidity 60±10%) with 12-h light/dark cycles, individually housed in polystyrene cages containing wood shavings and fed standard rodent chow and water *ad libitum*. All experiments were conducted with the approval of the Animal Care and Use Committee of Huazhong University of Science and Technology and were in accordance with the Guidelines of the National Institutes of Health Guide for the Care and Use of Laboratory Animals.

Bone cancer pain model

Rat BCP models were established as *per* the previous report with minor modifications(Guan et al., 2015b,). Briefly, Walker 256 mammary carcinoma cells were inoculated into the abdominal cavity of adult female SD rats and extracted from the ascites after 7 days, washed with D-Hank's solution and centrifuged at 500×*g* for 5 min at 4°C (5 cycles), and then calibrated at a concentration of 4×10^7 cells/mL and maintained on ice until inoculation. Under anesthesia with pentobarbital sodium (40 mg/kg, ip), rats were laid in the supine position, and the right legs were shaved and disinfected with 7% iodine. A small incision was made parallel to the tibia in order to expose the plateau. A 23-gauge needle was inserted into the tibial medullary canal to make a pathway for injecting carcinoma cells, which was replaced with a

10 μL Hamilton syringe. A 10-μL volume containing approximately 4×10^5 Walker 256 mammary carcinoma cells was slowly injected in the BCP group, while an equivalent volume of D-Hank's solution was injected into the sham rats. The injection site was sealed with bone wax as soon as the syringe was retracted, and the skin sutured with 4/0 thread (SA83G, Johnson & Johnson Medical (China) Ltd., Shanghai, China). All rats were placed on a warm pad until recovery from anesthesia and then transferred into their individual cages.

Bone radiological and histological detection

To analyze tibia bone destruction by Walker 256 carcinoma cells, bone radiography and histological staining were performed. Rats were placed on a clear plane plexiglass and exposed to an X-ray source under sodium pentobarbital anesthesia for 10 s at 25 kV_p. Lateral radiographs of the right tibia were acquired using a digital radiographer system (DR-F, GE, Atlanta, GA, USA). Based on the radiological results, the right tibias were then collected from euthanized rats for bone histological investigation. The bones were post-fixed with 4% paraformaldehyde (PFA) for 72 h, decalcified in 10% ethylenediaminetetraacetic acid (EDTA, pH=7.4) for 3 weeks, and decalcified in decalcifying solution for another 24 h. The tibias were washed, dehydrated, and embedded in paraffin, then cut into 5-μm sections and stained with hematoxylin and eosin to investigate carcinoma cell invasion and bone destruction.

Mechanical paw withdraw threshold test

As in previous reports(Dominguez et al., 2008; Guan et al., 2015b), mechanical allodynia was examined using the blind method. To avoid stress resulting from the test conditions, all rats were placed in a quiet test room for 5 d before basal measurements. Mechanical paw withdraw threshold (PWT) was measured using a series of calibrated von Frey filaments at

9:00 am. Rats were placed in plexiglass chambers with a wire net floor and were habituated for 30 min. A range of von Frey filaments (1-, 1.4-, 2-, 4-, 6-, 8-, 10-, and 15-g bending force; Stoelting, Wood Dale, IL, USA), starting with 1 g and ending with 15 g in ascending order, were applied to determine the mechanical PWT. The duration of each stimulus was maintained for approximately 1 s. Quick withdrawal or paw flinching was considered a positive response. Each monofilament was applied 5 times with a 30 s interval between applications, and the mechanical PWT was determined as the bending force of the filament for which at least 60% of the applications elicited a response.

Intrathecal catheter implantation, drug administration

Intrathecal cannula operation was performed as *per* previous reports. Briefly, rats were anesthetized with 2% isoflurane in 60% oxygen and intrathecally implanted with a polyethylene (PE)-10 catheter (inner diameter 0.3 mm, outer diameter 0.6 mm, PE-0503, Anilab Software & Instruments, Ningbo, China) through a gap in the vertebrae between L5 and L6 and extended to the subarachnoid space. Animals were allowed to recover for 3 days and then intrathecally injected with 1% lidocaine (10 μL) to confirm the catheter position. If any sign of nerve injury was observed, the rat was eliminated. The reagents minocycline (S4226), AG490 (S1143), Fludarabine (S1491), and U0126 (S1102) were purchased from Selleck Chemicals (Houston, U.S), and recombinant rat IFNγ (rrIFNγ) was obtained from PeproTech (400-20, Rocky Hill, NJ, USA). The dose we used here was based on previous reports(Dominguez et al., 2008; Guan et al., 2015a; Tsuda et al., 2009; Xu et al., 2015) and our preliminary results(Song et al., 2016). All reagents were freshly prepared in accordance with their respective instructions prior to each administration.

Lentivirus production and infection and spinal microinjection

Recombinant lentiviral vector expressing shRNA-CIITA to knockdown CIITA expression was obtained commercially from Genechem, Shanghai, China. The sense oligonucleotide for CIITA was 5'-TCAGGAGAGAAGCCTCAGA-3', and the antisense was 5'-TCTGAGGCTTCTCTCCTGA-3'; the two oligos were separated by a loop and inserted downstream of the U6 promoter in the lentiviral vector GV248. Lentiviruses were acquired from triple-infected 293T cells with approximately 80% confluence. The lentiviral vector backbone was hU6-MCS-Ubiquitin-EGFP-IRES-puromycin; in contrast, the same vector backbone without the shRNAs carrying eGFP was used as a negative control lentivirus (NC-LV). The viral titer for the stock was 6.0×10^8 TU/mL.

Lentiviral vectors were microinjected into the lumber spinal cord as *per* previous reports with minor modifications(Ke et al., 2016, 2013). Briefly, the rat's spine was stabilized with two individual bars fixed around the L3 vertebra under deep isoflurane anesthesia (2%). Under an operation microscope (Yihua Optical Apparatus Co. Ltd., Zhenjiang, China), the laminectomy of the thoracic T13 vertebra was gently and precisely performed to disclose the right side of the lumbar spinal cord. The intact dura mater and arachnoid mater were uncovered, and 2 μL (3.8×10^5 TU) of lentiviral vector was injected at a flow rate of 0.4 μL/min. The needle was positioned 0.4 mm to the right side of the dorsal midline and at a depth of 0.5 mm to reach the dorsal horn. After microinjection, the needle was left in place for an additional 5 min to prevent back flow. The same volume of NC-LV was injected in the control BCP rats. After muscle and skin were sutured with 4/0 stitches and disinfected with

7% iodine, rats were kept on a warm pad to recover. eGFP expression was examined by immunofluorescence to confirm successful lentiviral infection in each group.

Immunohistochemistry

After being deeply anesthetized with pentobarbital sodium (60 mg/kg, ip), rats were perfused through the ascending aorta with 300 mL of ice-cold saline, followed by 4% PFA in 0.1 M phosphate buffer (pH=7.35). The enlargement of the spinal cord (L2-L5) were collected, postfixed in the aforementioned fixative for 24 h at 4°C and cryoprotected in 30% sucrose for 48 h. Transverse sections (25-μm-thick) were cut on a cryostat (CM1900, Leica, Wiesbaden, Germany). Free-floating sections were washed in 3 times in PBS for 5 min each, penetrated with 0.3% TritonX-100 for 15 min and blocked with 5% bovine serum albumin (BSA) for 1 h at room temperature (23±2°C). For double immunofluorescence, sections were incubated with a mixture of two primary antibodies for 48 h at 4°C. Specifically, to confirm MHC II expression on microglia, mouse anti-MHC class II RT1B primary antibody (1:100, MCA46R, AbDSerotec, Kidlington, UK) was mixed with goat anti-Iba1 primary antibody (microglia biomarker, 1:200, ab5067, Abcam, Cambridge, UK). To identify the cell type expressing pSTAT1ser727, primary antibody for this protein (1:100, 9177, rabbit anti-pSTAT1ser727, Cell Signaling Technology, Danvers, MA, USA) was co-cultured with primary antibody against Iba1 (1:200, ab5067, Abcam), mouse anti-glial fibrillary acidic protein (anti-GFAP, astrocyte biomarker, 1:500, 3670, Cell Signaling Technology), or mouse anti-NeuN (neuronal biomarker, 1:200, MAB377, Merck Millipore, Darmstadt, Germany). After being washed three times with PBS, the free-floating sections were incubated in a mixture of secondary antibodies for 2 h at room temperature (23±2°C) if necessary – Cyanine Cy^{TM}3-conjugated

donkey-anti-mouse Ig (1:300, 715-165-150, Jackson ImmunoResearch, West Grove, PA, USA), Cyanine Cy^{TM}3-conjugated donkey-anti-rabbit Ig (1:300, 711-165-152, Jackson ImmunoResearch), Fluorescein (FITC)-conjugated donkey-anti-goat Ig (1:200, 705-095-003, Jackson ImmunoResearch), or Fluorescein (FITC)-conjugated donkey-anti-mouse Ig (1:200, 715-095-150, Jackson ImmunoResearch) – and mounted with Fluoromount-G solution (0100-01, SouthernBiotech, Birmingham, AL, USA). Images were captured on a Leica fluorescence microscope (DM2500, Mannheim, Germany) or a laser scanning confocal microscope (FV1000, Olympus, Tokyo, Japan).

Western blotting

Animals were rapidly perfused through the ascending aorta with 300 mL of ice-cold saline under pentobarbital sodium (60 mg/kg, ip) anesthesia, and L2-L5 spinal cord segments were collected and stored at -80°C. Total proteins were extracted on ice using lysis buffer (250.0 mM sucrose, 20.0 mM Tris, 0.03 mM Na_3VO_4, 2.0 mM $MgCl_2$, 2.0 mM EDTA, 2.0 mM EGTA, 2.0 mM phenylmethylsulfonyl fluoride, 1.0 mM dithiothreitol, 0.02% protease inhibitor cocktail; pH=7.4), and protein concentrations were determined using a BCA Protein Assay Kit (AR0146, Boster, Wuhan, China). The protein samples were heated in water for 10 min at 95°C with SDS-PAGE buffer; equal amounts of protein (20-50 μg) were then separated by 10% SDS-PAGE and subsequently electrotransferred onto polyvinylidene fluoride membranes (IPVH00010, Millipore, Billerica, MA, USA). The membranes were blocked with 5% BSA in TBST (0.1%) at room temperature (23±2°C) for 2 h, incubated overnight at 4°C with the indicated primary antibody, and then further incubated with horseradish peroxidase (HRP)-conjugated secondary antibodies for 2 h at room temperature.

The antibodies used in this study include mouse anti-MHC class II RT1B (1:500, MCA46R, AbDSerotec), rabbit anti-CIITA (1:500, sc-48797, Santa Cruz, Dallas, TX, USA), rabbit anti-pSTAT1ser727 (1:1000, 9177, Cell Signaling Technology), rabbit anti-STAT1(1:1000, 14994, Cell Signaling Technology, Danvers, MA, USA), rabbit anti-pERK1/2 Thr202/Tyr04 (1:1000, 4370, Cell Signaling Technology, Danvers, MA, USA), rabbit anti-ERK1/2 (1:1000, 9102, Cell Signaling Technology, Danvers, MA, USA), mouse anti-β-actin (1:500, BM0627, Boster, Wuhan, China), HRP-conjugated goat-anti-mouse (1:5000, P0008, Promoter, Wuhan, China) and goat-anti-rabbit secondary antibody (1:5000, P0009, Promoter, Wuhan, China). Target protein bands were visualized using chemiluminescence (Pierce ECL Western Blotting Substrate, 32209, Thermo Scientific) and measured by a computerized image analysis system (ChemiDoc XRS+, BIO-RAD, CA, USA).

Real-time quantitative PCR

Total RNA was extracted from rat spinal cords (L2-L5) using TRIzol reagent (Invitrogen, USA) according to the manufacturer's protocol and quantified using a spectrophotometer (BioPhotometer, Eppendorf, Hamburg, Germany). Quantitative real-time PCR was performed on a LightCycler system (StepOne, Applied Biosystems, Foster City, CA, USA) using SYBR green to detect amplification, and each sample was run in triplicate with 2 μL of reverse transcription product in a 25-μL reaction mixture. The data were analyzed with StepOne-Software-v2.0 (Applied Biosystems) using the standard curve method. GAPDH was used as an internal control. The reaction conditions for PCR were set up based on the manufacturer's protocol: incubation was set at 95°C for 3 min, followed by 40 cycles of 10 s at 95°C, 20 s at 58°C, and 10 s at 72°C. The threshold cycle (CT) was used to estimate the

amount of target mRNA. The comparative CT method with the formula for relative fold-change=$2^{-\Delta\Delta CT}$ was used to quantify the amplified transcripts. The specific primer sequences were designed and synthesized by Takara (Kyoto, Japan): CIITA - 5'-AACTGCATTGTGACGAAGG-3' (sense), 5'-CCGTGAACTTGTTGAACTGG-3' (antisense); STAT1 - 5'-CATCACATTCACATGGGTGG-3' (sense), 5'-ATTGGGATACAGATACTTCAGG-3' (antisense); GAPDH - 5'-GGCACAGTCAAGGCTGAGAATG-3'(sense), 5'-ATGGTGGTGAAGACGCCACTA-3' (antisense).

Primary microglia culture and investigation *in vitro*

Primary microglia were prepared by the shaking method from the cerebral cortex of 24-h-old rat pups as reported previously(Nikodemova et al., 2007). The cerebral cortex was dissected, minced, and trypsinized in 0.25% trypsin-EDTA for 20 min at 37°C. After the addition of horse serum to stop the reaction, the tissues were triturated with a Pasteur pipette and filtered consecutively through 70- and 45-μm pore-size nylon cell strainers. Collected cells were resuspended in Dulbecco's modified Eagle's medium supplemented with 10% fetal bovine serum and 100 U/mL penicillin/streptomycin and plated in 80-mm^2 tissue flasks. After10 days, the flasks were gently shaken for 1 h, and the medium was then harvested and centrifuged for 10 min at 1000×*g* to collect microglia. The cells were resuspended in the above medium and plated in 6-well plates at a density of 5×10^6 cells/well. For the control group, cells were treated with DMSO (0.1%) or rrIFNγ (10 ng/mL); for the interference step, cells were treated with AG490 (50 μM/mL), Fludarabine (50 μM/mL), and U0126 (30

μM/mL) for 30 min prior to interfering with the rrIFNγ. When the treatments were finished, cells were cultured for 24 h, and total proteins were prepared for western blot analyses.

Enzyme-linked immunosorbent assay (ELISA) for CXCL9 and CXCL11

Rat CXCL9 (Lot No. MDE96201608M) and CXCL11 (Lot No. MDE96201608T) ELISA Kits were purchased from MDL Biotech (Beijing, China). The spinal cords were homogenized in lysis buffer in order to extract the supernatant. The serum samples were prepared from rat whole blood by centrifugation at 3000×*g* for 10 min. ELISA was performed according to the manufacturer's protocol. Samples (10 μL) were added to the wells and diluted with 40 μL dilution buffer, after which the samples were incubated for 60 min at room temperature. After three washes with 200 μL of wash buffer, the plates were dried, zymolytes added, and the absorbance was measured on a spectrophotometer at 450 nm (Model 680, BIO-RAD, CA, USA). The readings were normalized to the amount of standard protein of each sample.

Statistics

Statistical analyses were performed using SPSS 17.0 (Chicago, IL, USA). All data are presented as the mean ± standard error of the mean (SEM). The differences were evaluated using unpaired Student's *t* tests to compare two groups or one-way analysis of variance (ANOVA) for multiple comparisons followed by Bonferroni or Dunnett's T3 tests if necessary. The differences in the mechanical PWT data between groups were analyzed *via* two-way ANOVA, in which "Time" was treated as the "within-subjects" factor and "Treatment" was treated as the "between-subjects" factor followed by Tukey *post hoc* tests. $P<0.05$ was considered to be statistically significant.

Results

Inoculation of Walker 256 mammary carcinoma cells induced bone cancer pain

In the present study, Walker 256 carcinoma cells were collected to establish a BCP rat model using intratibial-cavity injection. No radiological changes were observed in sham rats at day 21 following the sham operation compared with naive rats. In contrast, 7 days after tumor cell inoculation, the proximal epiphysis of the ipsilateral tibial bone (near the Walker 256 carcinoma cell injected site) showed signs of osteolytic destruction. Further deterioration was detected with both medullary and bicortical bone loss, pathological fracture was observed at days 14 and 21 in BCP rats, plus tumor cells had migrated out of the tibial cavity and into peripheral soft tissues at day 21 (Fig. 1A). Sections from bone histological investigation also revealed bone destruction in the ipsilateral tibia of BCP animals, which manifested as the time-dependent replacement normal of bone marrow cells by carcinoma cells and disappearance of healthy trabecular structures (Fig. 1B). The mechanical PWT was tested to assess BCP progression prior to (day 0) and at days 3, 7, 14, 17, and 21 following operation. The ipsilateral hindpaw of BCP rats displayed a dramatic decrease in mechanical PWT to von Frey filament stimulation from 10.78±0.42 g at baseline to 5.42±0.53 g after 7 days of inoculation and further deteriorated to 2.06±0.56 g at day 21. In contrast, no significant difference was observed among the sham rats (Fig. 1C). These data indicate the successful establishment of a BCP rat model by Walker 256 carcinoma cell inoculation in the present study.

MHC II was expressed on reactive spinal microglia in BCP rats

Microglia are regarded as the resident macrophage of the CNS and are involved in the development of BCP. Since the spinal cord dorsal horn has been identified as a major site for central sensitization(Kaan et al., 2010), the extent of microglia activation in the ipsilateral spinal dorsal horn was therefore investigated by immunofluorescence. The microglial cells in naive rats had small, rod-shaped somata and highly ramified extended processes, whereas those in the BCP rats were robustly activated, with hypertrophic somata and relatively short processes from day 14 after BCP induction. Moreover, the reactive microglia were robustly proliferated and clustered in the ipsilateral spinal cord at days 14 and 21 following Walker 256 carcinoma cell inoculation (Fig. 2B). MHC II in the spinal cord is likely to play an important role in mechanical hyperalgesia(Grace et al., 2011; Sweitzer et al., 2002); thus, the expression levels of CIITA and MHC II RT1B were examined by western blotting. CIITA expression was significantly increased by approximately two fold at day 7 (1.98±0.38-fold, $P<0.05$) and 14 (2.17±0.70-fold, $P<0.05$) in BCP rats yet decreased on day 21 (1.35±0.16-fold, $P=0.47$), although still remaining at a relatively high level. In addition, MCH II RT1B expression was upregulated at day 7 (2.45±0.69-fold, $P=0.29$), although without statistical significance, and peaked on day 14 (5.63±2.00-fold, $P<0.01$) after BCP induction and remained at high levels until the final examination on day 21 (4.03±1.62-fold, $P<0.01$). In contrast, no significant changes were observed in sham-operated rats compared with naive rats (Fig. 2A). We also determined whether MHC II RT1B was expressed exclusively on microglia under BCP conditions by double-immunofluorescence staining for MHC II RT1B and Iba1 (microglia biomarker), GFAP (astrocyte biomarker), or NeuN (neuron biomarker). Spinal samples acquired from naive and BCP rats indicated that MCH II

RT1B was co-expressed with Iba1-positive cells in the ipsilateral spinal dorsal horn (Fig. 2B), but not with GFAP or NeuN positive cells (data not shown). We found that Iba1(+)/MCH II RT1B(+) cells were predominantly allocated to the superficial dorsal horn of the spinal cord and upregulated in BCP rats from day 14 to day 21, consistent with the western blotting results. We next calculated the number of both Iba1- and MHC II RT1B-positive cells from lamina I to III and found that they were critically increased 14 days after BCP until the end of the observation period ($P<0.01$, Fig. 2C). These data indicate the importance of MHC II in the pathogenesis of BCP in the spinal cord.

Pharmacological and genetic downregulation of MHC II attenuated mechanical allodynia in BCP rats

To determine the role of MHC II in the progression of BCP, we pharmacologically and genetically modulated MHC II expression levels and examined mechanical PWT (Fig. 3A illustrates the experimental protocol). To reduce the number of experimental animals, we selected day 14 following BCP as the time point based on the above results. The prophylactic minocycline, which not only inhibits microglia but also downregulates microglial MHC II expression in microglia(Nikodemova et al., 2007), was intrathecally injected at a dose of 100 μg in 10 μL of saline once a day for 14 days beginning immediately after BCP induction. The results showed that minocycline effectively ameliorated the development of mechanical allodynia in the ipsilateral hindpaw (7.63±2.27 g *vs*2.73±0.62 g at day 10, $P<0.05$) and significantly inhibited MHC II RT1B expression (approximately three-fourths inhibition, $P<0.01$) in minocycline-treated BCP rats compared with the normal saline-treated group (Fig. 3B, C). CIITA is necessary for MHC II expression(Ting and Trowsdale, 2002); thus, to

further determine whether MHC II contributed to the development of BCP, a recombinant RNAi-LV conjugated with enhanced green fluorescent protein (eGFP) was microinjected into the ipsilateral spinal dorsal horn to knock down CIITA expression. As shown in Fig. 3D, the spread of lentiviral vectors was evaluated using transgene-produced eGFP, and the findings revealed that the lentivirus was mainly distributed in the L3 spinal cord dorsal horn and strictly restricted to the injected site. Fourteen days post Walker 256 carcinoma cell inoculation (11 days following microinjection), CIITA was examined by western blotting and RT-qPCR to test the efficiency of RNAi-LV. CIITA knockdown resulted in decreased MHC II RT1B and effectively attenuated tactile allodynia ($P<0.01$, Fig. 3E, F, G). Next, a potent MHC II inducer, rrIFNγ(Tsuda et al., 2009) was intrathecally injected (1000 U in 10 μL) into naive rats, as well as either RNAi-LV- or NC-LV-treated BCP rats (11 days post carcinoma cell inoculation). We found that rrIFNγ induced the reduction of mechanical PWT and significantly increased the expression of CIITA and MHC II RT1B in naive and NC-LV-treated BCP rats, but not in those treated with RNAi-LV, 72 h after intrathecal injection ($P<0.01$, Fig. 3H, I, J). These results further suggest that RNAi-LV effectively inhibited CIITA and MCH II RT1B in the lumbar spinal cord and confirm that MHC II is involved in mechanical allodynia. Taken together, these data demonstrate that MHC II mediates the mechanical allodynia underlying the BCP.

STAT1 and ERK are activated in the spinal cords of BCP rats

JAK/STAT1 signaling positively regulates MCH II expression by targeting CIITA(Ting and Trowsdale, 2002); we therefore examined the expression of total and activated STAT1 (pSTAT1ser727) in the spinal cord. Western blotting showed that pSTAT1ser727 accumulated

robustly in BCP rats after14 and 21days of carcinoma inoculation compared with naive rats (3.68±0.99-fold at day 14, 2.86±0.83-fold at day 21, $P<0.01$, Fig. 4A). Total STAT1 protein levels were also increased at day 7 (2.99±0.25-fold, $P<0.01$) and persisted until day 21 (2.47±0.19-fold at day 14, 2.59±0.38-fold at day 21). STAT1 mRNA level were also persistently increased in the BCP group compared with the naive group (3.65±0.21-fold at day 7, 4.16±0.29-fold at day 14, 2.75±0.11-fold at day 21, $P<0.01$, Fig. 4B), consistent with the western blot results. Moreover, immunofluorescence demonstrated that pSTAT1ser727 was expressed on both Iba1- and GFAP-positive cells but not on NeuN-positive cells (Fig. 4C). Previous work showed that ERK undergoes time-dependent phosphorylated in the spinal cord of BCP rats and is involved in mechanical hypersensitivity(Guan et al., 2015a). We also examined the time-course of ERK activation in the present study using western blotting and found that pERK was robustly increased at day 14 in cancer-bearing rats (1.59±0.18-fold, $P<0.01$) and persisted until day 21 (1.50±0.10-fold, $P<0.01$), consistent with the upregulation of pSTAT1ser727 (Fig. 5).

ERK regulates STAT1 phosphorylation and further modulates MHC II expression in the spinal cord

To investigate the role of STAT1 in BCP, AG490 (inhibitor of JAK, an upstream regulator of STAT1, 5 μg in 10 μL, it, once a day for 14 days) and Fludarabine (STAT1 inhibitor, 10 μg in 10 μL, it, once a day for 14 days) were prophylactically administered immediately after Walker 256 carcinoma cell inoculation for 14 consecutive days. As shown in Fig. 6A and B, pSTAT1ser727 was significantly inhibited by Fludarabine treatment ($P<0.01$) but not by AG490. Similarly, CIITA and MHC II RT1B expression levels were also inhibited by

Fludarabine (P<0.01, Fig. 6A, E, F), and mechanical allodynia was attenuated by this reagent (P<0.05 compared with control group, Fig. 5G). These data suggest that STAT1 phosphorylation might not be mainly activated by JAK and that pSTAT1 could be a prominent regulator of CIITA and MHC II expression in BCP. Furthermore, ERK signaling has been reported to interact with the JAK/STAT1 pathway(Dai et al., 2013; Gough et al., 2008; Li et al., 2010); therefore, we examined the relationship between ERK and JAK/STAT1 signaling under BCP conditions. A dose of 5 μg of the MEK inhibitor U0126 in 10 μL saline was intrathecally injected immediately following tumor cell inoculation for 14 consecutive days. The upregulation of pERK, pSTAT1ser727, CIITA, and MHC II RT1B were significantly inhibited by U0126 (P<0.05 compared with the control group, Fig. 6A, C, D～F), as was the mechanical PWT (P<0.05 compared with the control group, Fig. 6G). In particular, both AG490 and Fludarabine had relatively weaker effects on pERK levels (Fig. 6D). To identify the potency of AG490, we examined whether this reagent would inhibit IFNγ-induced STAT1 activation and ERK signaling. A dose of 5 μg of AG490 was injected into naive rats 30 min prior 1000 U of rrIFNγ, while the control group received only rrIFNγ. After 6 h, the enlargement of the spinal cord was collected, and the protein levels were examined by western blotting. The results showed that activated pSTAT1ser727 (P<0.05 compared with control group) and pERK (P<0.01 compared with control group) were dramatically inhibited by 5 μg of AG490; however, the total STAT1, CIITA, and MHC II RT1B did not differ significantly between the groups (Supplemental Fig, 1). Based on this evidence, we can reasonably conclude that the upregulation of pSTAT1ser727 occurred

mainly through ERK signaling in BCP rats, in other words, an alternative upstream molecule (not limited to JAK) regulated STAT1 phosphorylation in BCP.

ERK signaling regulates STAT1 phosphorylation to modulate MHC II expression on cultured primary microglia

pERK expression was previously reported in both spinal microglia and astrocytes in BCP rats(Wang et al., 2012). However, our current results demonstrated that pSTAT1 is also coexpressed in these glial cells, which led us to question how signaling modulates MHC II expression in microglia. Thus, we cultured primary microglial cells from the cerebral cortex of neonatal rat pups *in vitro* to further investigate the precise intracellular relationship between ERK and STAT1 signaling in modulating MHC II expression. In the presence of U0126, but not AG490, the upregulation of pSTAT1, pERK, CIITA, and MHC II RT1B in cultured cells induced with rrIFNγ was significantly inhibited ($P<0.05$ compared with the rrIFNγ stimulated group, Fig. 7A, B, D～F). Notably, Fludarabine exclusively inhibited upregulation of pSTAT1, CIITA, and MHC II RT1B expression ($P<0.05$ compared with the rrIFNγ stimulated group, Fig. 7A～C, F). These data are similar to the *in vivo* results, which further confirm that ERK signaling regulates STAT1 phosphorylation to modulate MHC II expression in microglia.

Possible extracellular triggers of ERK signaling pathway activation

Our previous study revealed that the activation of the chemokine receptor CXCR3 mediates BCP *via* the ERK signaling pathway(Guan et al., 2015a). We already investigated the chemokine CXCL10, one of three CXCR3 ligands, in another previous study(Bu et al., 2014); therefore, in the present study, we examined the expression levels of CXCL9 and CXCL11 in

the spinal cord or serum after BCP by ELISA. The results showed that spinal CXCL9 significantly increased 7 days after BCP and persisted for up to 21 days (P<0.01 compared with the naive group, Fig. 8A). For comparison, serum CXCL9 levels did not dramatically increase at any time point after BCP and even decreased at day 14 (P<0.05 compared with the naive group, Fig. 8B). CXCL11 levels did not change significantly in either the spinal cord or the serum, although they were slightly increased compared with naive rats (Fig. 8C, D). Our findings and those from previous studies suggest that the chemokines CXCL9 and CXCL10 may be possible extracellular signals that induce the activation of ERK signaling in spinal dorsal microglia under BCP conditions.

Discussion

In the current study, we demonstrated that (i) spinal dorsal horn microglia undergo proliferation after Walker 256 mammary carcinoma cell inoculation in SD rats; (ii) MHC II is expressed by activated microglia and contributes to the progression of bone cancer pain; (iii) STAT1 signaling is involved in the modulation of MHC II expression; and (iv) phosphorylation of STAT1 is regulated by ERK via a noncanonical pathway in microglia.

In recent decades, the development of BCP models has promoted progress in the investigation of BCP mechanisms. According to a review by Currie and colleagues(Currie et al., 2013), various carcinoma cell lines have been injected into mouse or rat axonal bones to mimic the symptoms and pathological features of clinical patients with BCP. In the present study, Walker 256 carcinoma cells were inoculated into the tibial cavity (consistent with previous methods(Bu et al., 2014; Guan et al., 2015a,)), which induced osteolysis, pathologic fracture, and mechanical allodynia. Therefore, a rat BCP model was successfully established.

Mounting evidence indicates that spinal cord microglia plays a crucial role in the development and maintenance of BCP(Hald et al., 2009; Lan et al., 2010; Zhang et al., 2005). Indeed, activated microglia interact with neurons by releasing a variety of pro-inflammatory cytokines, chemokines and neuronal mediators, resulting in central sensitization(Calvo and Bennett, 2012). The development of microgliosis in the CNS is a major contributor to the progression of chronic pain states, including neuropathic, inflammatory, and bone cancer pain(Calvo and Bennett, 2012). In our study, we found that activated microglia with bulk somata were distributed ipsilaterally in the spinal dorsal horn of BCP rats starting at 14 days following Walker 256 carcinoma cell inoculation and lasting until 21 days. The time-course

of prominent microglia proliferation correlated with the maintenance of BCP, which suggests that the role of microglia is not just limited to the initial phase of behavioral hypersensitivity. Of course, other factors such as inflammation, products secreted from the solid carcinoma, and tumor-induced injury to primary afferent neurons and bone remodeling cannot be excluded in the pathogenesis of BCP(Bloom et al., 2011; Clohisy and Mantyh, 2003). Remarkably, some of the microglia clustered and formed several colonies, potentially implying that these cells were chemotactic and migrated and were possibly involved in phagocytosis. Whether synaptic stripping, a process in which microglia selectively remove synapses from injured neurons(Trapp et al., 2007), underlies BCP is still far from certain, and this phenomenon requires further investigation.

Rat MHC gene sequences are located on the short arm of chromosome 20 and span approximately 4 Mb(Hurt et al., 2004). The effect of MHC was previously thought to be limited to antigen presentation; however, genetic studies have revealed that MHC is involved in basal pain perception, analgesia sensitivity, and chronic pain states(Dominguez et al., 2008; Mogil, 2012; Sato-Takeda et al., 2006). Furthermore, MHC II, which is not constitutively expressed in resting microglia, was shown to be potently upregulated as the cells are activated(Hamo et al., 2007). Sweitzer and colleagues demonstrated that MHC II-positive cells increased after peripheral nerve injury; similarly, MHC II knockout mice exhibited dramatically attenuated allodynia compared to their wild-type counterparts following L5 spinal nerve transection(Sweitzer and DeLeo, 2002; Sweitzer et al., 2002). In addition, an MHC haplotype involved in the incidence of post-herpetic pain has also been reported(Sato-Takeda et al., 2006). More recently, another group found that MHC II

contributes to differences in basal pain sensitivity and nociceptive responses in a formalin-induced pain model(Guo et al., 2010, 2015). However, MHC II has yet to be linked to BCP.

In the present study, we examined the expression of MHC II RT1B, synonymous with MHC II-DQ, and observed increased expression specifically in spinal microglia after 14 days of tumor cell inoculation, which correlates with the progression of mechanical allodynia. MHC II RT1B pharmacological inhibition and genetic interference both prevented tactile allodynia. Within the spinal cord, IFNγ receptors are specifically expressed by microglia, and intrathecal injection of rrIFNγ in normal animals produced tactile allodynia(Tsuda et al., 2009). More remarkably, this cytokine is the most effective activator of microglial MHC II expression(Hanna and Etzioni, 2014; Schartner et al., 2005), being most likely produced by astrocytes and neurons(Racz et al., 2008). When animals were intrathecally administered with rrIFNγ, upregulated MHC II expression, as well as mechanical allodynia, were observed in naive and NC-LV-treated rats but not in RNAi-LV-treated BCP rats. To our knowledge, this is the first report to identify a role for MCH II in the pathogenesis of BCP. These results suggest that MHC II is at least partly involved in the development and maintenance of BCP in rats.

CIITA can be divided into four general domains based on its structure, and the amino-terminal region functions as a transcriptional activator that interacts with many proteins. Three promoters (PI, PII, and PIV) control CIITA expression in a tissue-specific manner(Muhlethaler-Mottet et al., 1997). Notably, a growing body of evidence has unequivocally suggested that PIV CIITA expression requires STAT1(Levy and Darnell, 2002; Londhe and Davie, 2011; Morris et al., 2002; Muhlethaler-Mottet et al., 1998). CIITA is the

major transcriptional regulator of MHC II(Ting and Trowsdale, 2002), and CIITA deficiency results in a lack of MHC II expression in some cell types(Hanna and Etzioni, 2014). Activation of specific intracellular signaling pathways that modulate CIITA transcription, including STAT1, induces MHC II expression(Piskurich et al., 1999). STAT1 resides in the cytoplasm in resting cells, whereas it accumulates in the nucleus to drive transcription when activated(Levy and Darnell Jr, 2002). Interestingly, STAT1 tyrosine 701 phosphorylation is involved in DNA binding and transcription, while serine 727 phosphorylation initiates gene transactivation(Stark and Darnell Jr, 2012; Wang et al., 2015). In other words, full STAT1 transcriptional activity required phosphorylation at serine 727(Decker and Kovarik, 2000; Herrera-Molina et al., 2012; Kovarik et al., 2001; Stark and Darnell Jr, 2012). Moreover, emerging evidence suggests that serine727 phosphorylation is independently responsible for STAT1 transcriptional function(Liu et al., 2003; Ng et al., 2006). Some studies have reported that activated STAT1 binds to the CIITA promoter (Londhe and Davie, 2011; Morris et al., 2002; Piskurich et al., 1999, 1998). In the present study, we demonstrated that pSTAT1ser727 in microglia contributes to BCP in Walker 256 carcinoma cell-inoculated rats. Although the administration of AG490, a JAK inhibitor, did not block STAT1 phosphorylation, the effects of Fludarabine on CIITA and MHC II expression, as well as on mechanical allodynia, were more profound. In the basic model of STAT1 activation, tyrosine 701 phosphorylation is regarded as a perquisite for serine 727 phosphorylation(Herrera-Molina et al., 2012); however, emerging evidence indicates that serine 727 can be phosphorylated by other kinases or signal transducers(Decker and Kovarik, 2000; Ng et al., 2006). Nevertheless, the partly selective

inhibitory function of AG490 on JAK cannot be entirely excluded. Therefore, alternative upstream molecule(s) for STAT1 serine 727 phosphorylation may be involved in BCP.

A previous report suggested that activated ERK is involved in BCP(Guan et al., 2015a), and others have also shown that STAT1 can be activated by ERK(Dai et al., 2013; Wang et al., 2010); thus, we postulated that ERK is responsible for STAT1 activation. In the present study, tumor-bearing rats treated with U0126 showed significant inhibition of pSTAT1ser727. The JAK inhibitor AG490 had weaker inhibitory effects on pSTAT1ser727 and pERK but suppressed IFNγ-induced signaling activation, which further confirmed that STAT1 signaling is not triggered by its canonical upstream molecule JAK under BCP conditions. These results suggest that ERK-dependent factors play an important role in STAT1 phosphorylation and in the development and maintenance of BCP in rats. In addition, the upregulation of CIITA and MHC II expression underlying BCP was reduced by U0126. Indeed, both ERK and STAT are downstream of gp130 in the intracellular signaling network. Furthermore, STAT proteins contain highly conserved phosphorylation sites for ERK(Dai et al., 2013). During the development of tolerance to morphine-induced analgesia as well as other cell types stimulated by IFNγ, STAT1 phosphorylation at serine727, but not at tyrosine701, was shown to be dependent on ERK(Wang et al., 2010; Wen et al., 1995), which is consistent with our current findings. Other studies have also shown that crosstalk between ERK and STAT1 depends on serine727 phosphorylation, with the two signaling pathways synergistically mediating intracellular signal transduction(Kovarik et al., 2001; Tian et al., 2004). Since the inhibitory effects of both AG490 and Fludarabine on pERK were not as profound as those of

U0126 in our BCP model, we speculate that this discrepancy can be attributed to differences in the cell types and pathophysiological conditions, which thus warrants further exploration.

As demonstrated previously, pERK was expressed in both microglia and astrocytes in BCP in which the same carcinoma cell line and animal species as ours were adopted(Wang et al., 2012). Phosphorylated STAT1 was also observed to co-localize with these two different types of glial cells in the present study. Unfortunately, we could not clearly determine how this signaling pathway regulates MHC II expression due to the complex relationship between microglia and astrocytes *in vivo*. Therefore, to further identify the specific roles of and relationship between the intracellular signaling pathways in these two cell types, we cultured primary cerebral cortex microglia from rat pups *in vitro*. Previous studies reported that IFNγ not only induces microglial activation(Graeber, 2010; Smith, 2010; Tsuda et al., 2009) but also activates CIITA transcription(Ting and Trowsdale, 2002). Therefore, this cytokine was selectively used to stimulate cultured primary microglia. As predicted, the results mirror those obtained in animals.

The CNS is not a completely privileged immunological organ since an immune can develop under certain conditions. This knowledge is completely confirmed by the recent discovery of the structural and functional features of central nervous system lymphatic vessels(Louveau et al., 2015). In some autoimmune diseases such as multiple sclerosis, as well as in injury-induced neuropathic pain, peripheral $CD4^+$ T lymphocytes that infiltrate through the blood-brain barrier can interact with microglia and release pro-inflammatory cytokines(Calvo et al., 2012; Cao and DeLeo, 2008; Chastain et al., 2011; Grace et al., 2011). A review by Grace et al. highlighted the role of immunological synapses between MHC

II-positive microglia and $CD4^+$ T lymphocytes in the pathogenesis of neuropathic pain(Grace et al., 2011). In this respect, we speculate that BCP is not an exception since peripheral immune cells could migrate into the spinal cord to interact reciprocally with spinal microglia. Alternatively, infiltrated $CD4^+$ T lymphocytes might interact with MHC II-presented antigens and contribute to the development and maintenance of BCP. However, this hypothesis should be carefully investigated.

Intracellular signaling pathways act as a point of convergence between extracellular signals and the intracellular events underlying physiological and pathological conditions. A wealth of evidence has suggested that phosphorylated ERK is an important intracellular signal in the development of bone cancer pain(Wang et al., 2011; Wang et al., 2012). However, there is little evidence to suggest which extracellular signals induce the activation of ERK signaling in spinal dorsal microglia in BCP. Our results suggest that the chemokines CXCL9 and CXCL10 are involved in the activation of intracellular ERK signaling *via* their common receptor CXCR3. Because microglia have receptors for and respond to injury signals such as cytokines and other chemokines (CCL2, Fractalkine, IFNγ, *etc.*), multiple factors can induce the activation of ERK signaling *via* these receptors. The extracellular signals that trigger ERK activation in BCP therefore require further study.

In summary (Fig. 9), the present study demonstrated that STAT1 is a downstream mediator of ERK signaling that contributes to bone cancer pain by regulating MHC II expression in spinal microglia. Moreover, STAT1 is expressed in spinal microglia and astrocytes under BCP conditions.

Acknowledgments

The work was supported by National Natural Science Foundation of China, Beijing, China (No. 81371250, 81400917, 81571053, 81660200, and 81460176).

Competing interests

The authors declare no competing interests.

Author contribution

Zhenpeng Song and Bingrui Xiong designed the experiments and performed the animal surgery, behavioral testing, immunohistochemistry, and Western blotting analyses. Anne Manyande and Fei Cao wrote the paper and analyzed the data. Hua Zheng and Yaqun Zhou carried out the cell culture. Xuehai Guan and Lifang Ren performed the real time quantitative PCR. Yuke Tian and Dawei Ye conceived the project, coordinated and supervised the experiments, and revised the manuscript.

References

Bloom AP, Jimenez-Andrade JM, Taylor RN, Castañeda-Corral G, Kaczmarska MJ, Freeman KT, Coughlin KA, Ghilardi JR, Kuskowski MA, Mantyh PW (2011) Breast cancer-induced bone remodeling, skeletal pain, and sprouting of sensory nerve fibers. J Pain 12:698-711.

Bu H, Shu B, Gao F, Liu C, Guan X, Ke C, Cao F, Hinton AO, Xiang H, Yang H, Tian X, Tian Y (2014) Spinal IFN-γ-induced protein-10 (CXCL10) mediates metastatic breast cancer-induced bone pain by activation of microglia in rat models. Breast Cancer Res Treat 143:255-263.

Calvo M, Bennett DL (2012) The mechanisms of microgliosis and pain following peripheral nerve injury. Exp Neurol 234:271-282.

Calvo M, Dawes JM, Bennett DL (2012) The role of the immune system in the generation of neuropathic pain. Lancet Neurol 11:629-642.

Cao L, DeLeo JA (2008) CNS-infiltrating CD4+ T lymphocytes contribute to murine spinal nerve transection-induced neuropathic pain. Eur J Immunol 38:448-458.

Chastain EM, Duncan DS, Rodgers JM, Miller SD (2011) The role of antigen presenting cells in multiple sclerosis. Biochim Biophys Acta 1812:265-274.

Clohisy DR, Mantyh PW (2003) Bone cancer pain. Cancer 97:866-873.

Currie GL, Delaney A, Bennett MI, Dickenson AH, Egan KJ, Vesterinen HM, Sena ES, Macleod MR, Colvin LA, Fallon MT (2013) Animal models of bone cancer pain: systematic review and meta-analyses. Pain 154:917-926.

Dai B, Cui M, Zhu M, Su WL, Qiu MC, Zhang H (2013) STAT1/3 and ERK1/2 synergistically regulate cardiac fibrosis induced by high glucose. Cell Physiol Biochem

32:960-971.

Decker T, Kovarik P (2000) Serine phosphorylation of STATs. Oncogene 19:2628-2637.

Dominguez CA, Lidman O, Hao JX, Diez M, Tuncel J, Olsson T, Wiesenfeld-Hallin Z, Piehl F, Xu XJ (2008) Genetic analysis of neuropathic pain-like behavior following peripheral nerve injury suggests a role of the major histocompatibility complex in development of allodynia. Pain 136:313-319.

Dominguez E, Rivat C, Pommier B, Mauborgne A, Pohl M (2008) JAK/STAT3 pathway is activated in spinal cord microglia after peripheral nerve injury and contributes to neuropathic pain development in rat. J Neurochem 107:50-60.

Gough DJ, Levy DE, Johnstone RW, Clarke CJ (2008) IFNgamma signaling-does it mean JAK-STAT. Cytokine Growth Factor Rev 19:383-394.

Grace PM, Rolan PE, Hutchinson MR (2011) Peripheral immune contributions to the maintenance of central glial activation underlying neuropathic pain. Brain Behav Immun 25:1322-1332.

Graeber MB (2010) Changing face of microglia. Science 330:783-788.

Guan XH, Fu QC, Shi D, Bu HL, Song ZP, Xiong BR, Shu B, Xiang HB, Xu B, Manyande A, Cao F, Tian YK (2015a) Activation of spinal chemokine receptor CXCR3 mediates bone cancer pain through an Akt-ERK crosstalk pathway in rats. Exp Neurol 263:39-49.

Guan X, Fu Q, Xiong B, Song Z, Shu B, Bu H, Xu B, Manyande A, Cao F, Tian Y (2015b) Activation of PI3Kγ/Akt pathway mediates bone cancer pain in rats. J Neurochem 134:590-600.

Guo Y, Yao F, Lu S, Cao DY, Reed WR, Zhao Y (2010) The major histocompatibility

complex genes are associated with basal pain sensitivity differences between Dark-Agouti and novel congenic DA.1U rats. Life Sci 86:972-978.

Guo Y, Yao FR, Cao DY, Li L, Wang HS, Xie W, Zhao Y (2015) The major histocompatibility complex genes impact pain response in DA and DA.1U rats. Physiol Behav 147:30-37.

Hald A, Nedergaard S, Hansen RR, Ding M, Heegaard AM (2009) Differential activation of spinal cord glial cells in murine models of neuropathic and cancer pain. Eur J Pain 13:138-145.

Hamo L, Stohlman SA, Otto-Duessel M, Bergmann CC (2007) Distinct regulation of MHC molecule expression on astrocytes and microglia during viral encephalomyelitis. Glia 55:1169-1177.

Hanisch UK, Kettenmann H (2007) Microglia: active sensor and versatile effector cells in the normal and pathologic brain. Nat Neurosci 10:1387-1394.

Hanna S, Etzioni A (2014) MHC class I and II deficiencies. J Allergy Clin Immunol 134:269-275.

Hashizume H, Rutkowski MD, Weinstein JN, DeLeo JA (2000) Central administration of methotrexate reduces mechanical allodynia in an animal model of radiculopathy/sciatica. Pain 87:159-169.

Herrera-Molina R, Flores B, Orellana JA, von BR (2012) Modulation of interferon-gamma-induced glial cell activation by transforming growth factor beta1: a role for STAT1 and MAPK pathways. J Neurochem 123:113-123.

Hurt P, Walter L, Sudbrak R, Klages S, Müller I, Shiina T, Inoko H, Lehrach H, Günther E, Reinhardt R, Himmelbauer H (2004) The genomic sequence and comparative analysis of the

rat major histocompatibility complex. Genome Res 14:631-639.

Kaan TK, Yip PK, Patel S, Davies M, Marchand F, Cockayne DA, Nunn PA, Dickenson AH, Ford AP, Zhong Y, Malcangio M, McMahon SB (2010) Systemic blockade of P2X3 and P2X2/3 receptors attenuates bone cancer pain behaviour in rats. Brain 133:2549-2564.

Ke C, Gao F, Tian X, Li C, Shi D, He W, Tian Y (2016) Slit2/Robo1 Mediation of Synaptic Plasticity Contributes to Bone Cancer Pain. Mol Neurobiol .

Ke C, Li C, Huang X, Cao F, Shi D, He W, Bu H, Gao F, Cai T, Hinton AO, Tian Y (2013) Protocadherin20 promotes excitatory synaptogenesis in dorsal horn and contributes to bone cancer pain. Neuropharmacology 75:181-190.

Kovarik P, Mangold M, Ramsauer K, Heidari H, Steinborn R, Zotter A, Levy DE, Muller M, Decker T (2001) Specificity of signaling by STAT1 depends on SH2 and C-terminal domains that regulate Ser727 phosphorylation, differentially affecting specific target gene expression. EMBO J 20:91-100.

Lan LS, Ping YJ, Na WL, Miao J, Cheng QQ, Ni MZ, Lei L, Fang LC, Guang RC, Jin Z, Wei L (2010) Down-regulation of Toll-like receptor 4 gene expression by short interfering RNA attenuates bone cancer pain in a rat model. Mol Pain 6:2.

Levy DE, Darnell JE Jr (2002) Stats: transcriptional control and biological impact. Nat Rev Mol Cell Biol 3:651-662.

Li N, McLaren JE, Michael DR, Clement M, Fielding CA, Ramji DP (2010) ERK is integral to the IFN-γ-mediated activation of STAT1, the expression of key genes implicated in atherosclerosis, and the uptake of modified lipoproteins by human macrophages. J Immunol 185:3041-3048.

Lincoln MR, Montpetit A, Cader MZ, Saarela J, Dyment DA, Tiislar M, Ferretti V, Tienari PJ, Sadovnick AD, Peltonen L, Ebers GC, Hudson TJ (2005) A predominant role for the HLA class II region in the association of the MHC region with multiple sclerosis. Nat Genet 37:1108-1112.

Liu H, Ma Y, Cole SM, Zander C, Chen KH, Karras J, Pope RM (2003) Serine phosphorylation of STAT3 is essential for Mcl-1 expression and macrophage survival. Blood 102:344-352.

Londhe P, Davie JK (2011) Gamma interferon modulates myogenesis through the major histocompatibility complex class II transactivator, CIITA. Mol Cell Biol 31:2854-2866.

Louveau A, Smirnov I, Keyes TJ, Eccles JD, Rouhani SJ, Peske JD, Derecki NC, Castle D, Mandell JW, Lee KS, Harris TH, Kipnis J (2015) Structural and functional features of central nervous system lymphatic vessels. Nature 523:337-341.

Mogil JS (2012) Pain genetics: past, present and future. Trends Genet 28:258-266.

Morris AC, Beresford GW, Mooney MR, Boss JM (2002) Kinetics of a gamma interferon response: expression and assembly of CIITA promoter IV and inhibition by methylation. Mol Cell Biol 22:4781-4791.

Muhlethaler-Mottet A, Otten LA, Steimle V, Mach B (1997) Expression of MHC class II molecules in different cellular and functional compartments is controlled by differential usage of multiple promoters of the transactivator CIITA. EMBO J 16:2851-2860.

Muhlethaler-Mottet A, Di BW, Otten LA, Mach B (1998) Activation of the MHC class II transactivator CIITA by interferon-gamma requires cooperative interaction between Stat1 and USF-1. Immunity 8:157-166.

Ng YP, Cheung ZH, Ip NY (2006) STAT3 as a downstream mediator of Trk signaling and functions. J Biol Chem 281:15636-15644.

Nikodemova M, Watters JJ, Jackson SJ, Yang SK, Duncan ID (2007) Minocycline down-regulates MHC II expression in microglia and macrophages through inhibition of IRF-1 and protein kinase C (PKC)alpha/betaII. J Biol Chem 282:15208-15216.

Nimmerjahn A, Kirchhoff F, Helmchen F (2005) Resting microglial cells are highly dynamic surveillants of brain parenchyma in vivo. Science 308:1314-1318.

Piskurich JF, Linhoff MW, Wang Y, Ting JP (1999) Two distinct gamma interferon-inducible promoters of the major histocompatibility complex class II transactivator gene are differentially regulated by STAT1, interferon regulatory factor 1, and transforming growth factor beta. Mol Cell Biol 19:431-440.

Piskurich JF, Wang Y, Linhoff MW, White LC, Ting JP (1998) Identification of distinct regions of 5' flanking DNA that mediate constitutive, IFN-gamma, STAT1, and TGF-beta-regulated expression of the class II transactivator gene. J Immunol 160:233-240.

Racz I, Nadal X, Alferink J, Banos JE, Rehnelt J, Martin M, Pintado B, Gutierrez-Adan A, Sanguino E, Bellora N, Manzanares J, Zimmer A, Maldonado R (2008) Interferon-gamma is a critical modulator of CB(2) cannabinoid receptor signaling during neuropathic pain. J Neurosci 28:12136-12145.

Roche PA, Furuta K (2015) The ins and outs of MHC class II-mediated antigen processing and presentation. Nat Rev Immunol 15:203-216.

Sato-Takeda M, Takasaki I, Takeda K, Sasaki A, Andoh T, Nojima H, Shiraki K, Kuraishi Y, Hanaoka K, Tokunaga K, Yabe T (2006) Major histocompatibility complex haplotype is

associated with postherpetic pain in mice. Anesthesiology 104:1063-1069.

Schartner JM, Hagar AR, Van Handel M, Zhang L, Nadkarni N, Badie B (2005) Impaired capacity for upregulation of MHC class II in tumor-associated microglia. Glia 51:279-285.

Selvaraj D, Gangadharan V, Michalski CW, Kurejova M, Stösser S, Srivastava K, Schweizerhof M, Waltenberger J, Ferrara N, Heppenstall P, Shibuya M, Augustin HG, Kuner R (2015) A Functional Role for VEGFR1 Expressed in Peripheral Sensory Neurons in Cancer Pain. Cancer Cell 27:780-796.

Siegel RL, Miller KD, Jemal A (2016) Cancer statistics, 2016. CA Cancer J Clin 66:7-30.

Smith HS (2010) Activated microglia in nociception. Pain Physician 13:295-304.

Song ZP, Xiong BR, Guan XH, Cao F, Manyande A, Zhou YQ, Zheng H, Tian YK (2016) Minocycline attenuates bone cancer pain in rats by inhibiting NFκB in spinal astrocytes. Acta Pharmacol Sin 37: 753-762.

Stark GR, Darnell JE Jr (2012) The JAK-STAT pathway at twenty. Immunity 36:503-514.

Sweitzer SM, DeLeo JA (2002) The active metabolite of leflunomide, an immunosuppressive agent, reduces mechanical sensitivity in a rat mononeuropathy model. J Pain 3:360-368.

Sweitzer SM, White KA, Dutta C, DeLeo JA (2002) The differential role of spinal MHC class II and cellular adhesion molecules in peripheral inflammatory versus neuropathic pain in rodents. J Neuroimmunol 125:82-93.

Tian ZJ, Cui W, Li YJ, Hao YM, Du J, Liu F, Zhang H, Zu XG, Liu SY, Chen L, An W (2004) Different contributions of STAT3, ERK1/2, and PI3-K signaling to cardiomyocyte hypertrophy by cardiotrophin-1. Acta Pharmacol Sin 25:1157-1164.

Ting JP, Trowsdale J (2002) Genetic control of MHC class II expression. Cell 109

Suppl:S21-33.

Trapp BD, Wujek JR, Criste GA, Jalabi W, Yin X, Kidd GJ, Stohlman S, Ransohoff R (2007) Evidence for synaptic stripping by cortical microglia. Glia 55:360-368.

Tsuda M, Masuda T, Kitano J, Shimoyama H, Tozaki-Saitoh H, Inoue K (2009) IFN-gamma receptor signaling mediates spinal microglia activation driving neuropathic pain. Proc Natl Acad Sci U S A 106:8032-8037.

Wang LN, Yao M, Yang JP, et al. Cancer-induced bone pain sequentially activates the ERK/MAPK pathway in different cell types in the rat spinal cord. Mol Pain. 2011. 7: 48.

Wang S, Patsis C, Koromilas AE (2015) Stat1 stimulates cap-independent mRNA translation to inhibit cell proliferation and promote survival in response to antitumor drugs. Proc Natl Acad Sci U S A 112:E2149-2155.

Wang XW, Li TT, Zhao J, Mao-Ying QL, Zhang H, Hu S, Li Q, Mi WL, Wu GC, Zhang YQ, Wang YQ (2012) Extracellular signal-regulated kinase activation in spinal astrocytes and microglia contributes to cancer-induced bone pain in rats. Neuroscience 217:172-181.

Wang Z, Ma W, Chabot JG, Quirion R (2010) Calcitonin gene-related peptide as a regulator of neuronal CaMKII-CREB, microglial p38-NFkappaB and astroglial ERK-Stat1/3 cascades mediating the development of tolerance to morphine-induced analgesia. Pain 151:194-205.

Wen Z, Zhong Z, Darnell JE Jr (1995) Maximal activation of transcription by Stat1 and Stat3 requires both tyrosine and serine phosphorylation. Cell 82:241-250.

Xu Q, Jiang C, Rong Y, Yang C, Liu Y, Xu K (2015) The effects of fludarabine on rat cerebral ischemia. J Mol Neurosci 55:289-296.

Zhang RX, Liu B, Wang L, Ren K, Qiao JT, Berman BM, Lao L (2005) Spinal glial

activation in a new rat model of bone cancer pain produced by prostate cancer cell inoculation of the tibia. Pain 118:125-136.

Zhou X, Zoller T, Krieglstein K, Spittau B (2015) TGFbeta1 inhibits IFNgamma-mediated microglia activation and protects mDA neurons from IFNgamma-driven neurotoxicity. J Neurochem 134:125-134.

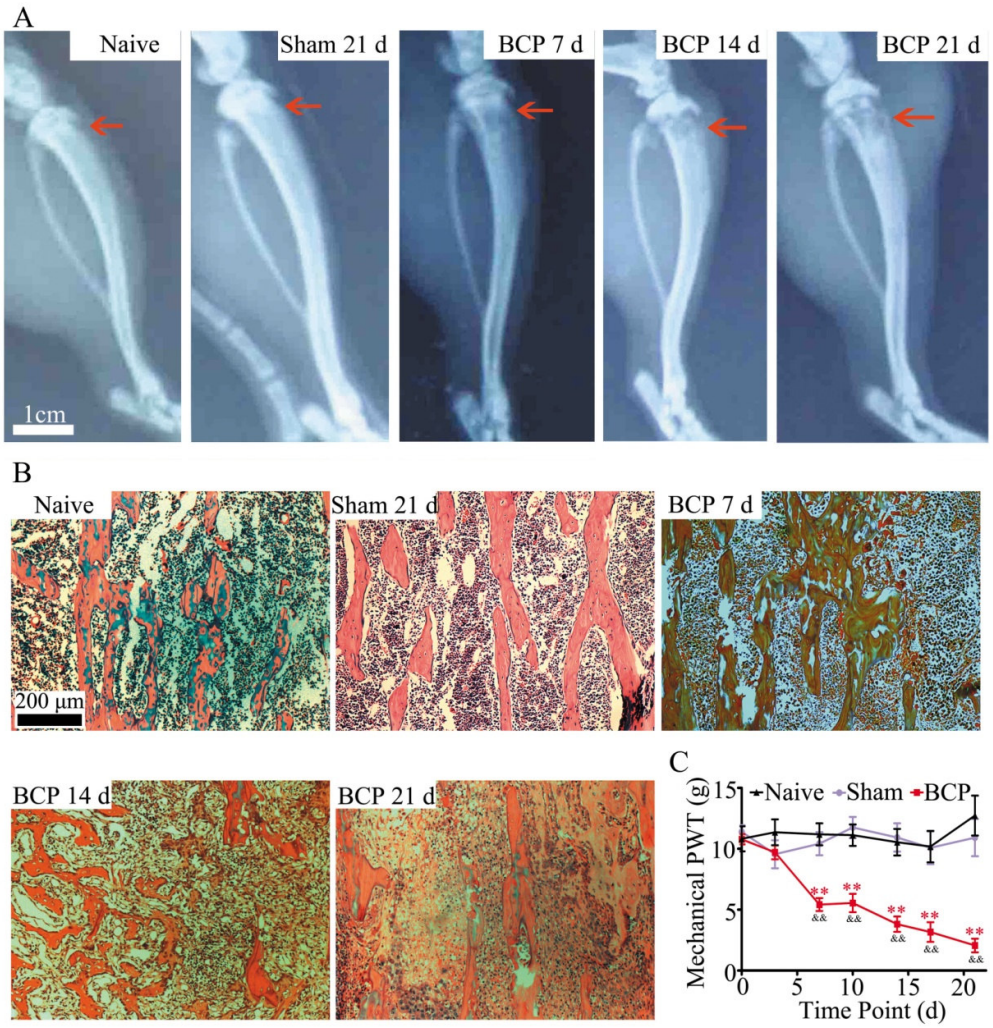

Fig. 1. Inoculation of Walker 256 carcinoma cells induced tibial osteolysis and mechanical allodynia. (A) Radiological results demonstrate signs of osteolytic destruction in the proximal epiphysis of the ipsilateral tibia (red arrow) in a time-dependent manner, with some carcinoma cells also migrating out of the tibial cavity and damaging the peripheral soft tissues at day 21; no significant changes were observed in naive and sham (21 days following sham operation) rats (*n*=3 rats for each group). Scale bar=1 cm. (B) HE-stained sections show normal trabecular structure and marrow cells in naive and sham (21 days following sham operation) rats; in contrast, the normal marrow cells were replaced by inoculated Walker 256

carcinoma cells and healthy bone structure disappeared starting from day 14 (n=3 rats in each group). Scale bar=200 μm. (C) Mechanical paw withdrawal threshold (PWT) was tested using a series of calibrated von Frey filaments prior to tumor cell inoculation (0 day) and at 3, 7, 10, 14, 17, and 21 days following model operation. The results are expressed as the mean±SEM, showing that the mechanical PWT decreased from 10.78±0.42 g at baseline to 5.42±0.53 g at day 7 and further deteriorated to 2.06±0.56 g at day 21 post-inoculation in the BCP group. $^{**}P<0.01$ compared with the baseline in each group; $^{\&\&}P<0.01$ compared with the naive group at each corresponding time point.

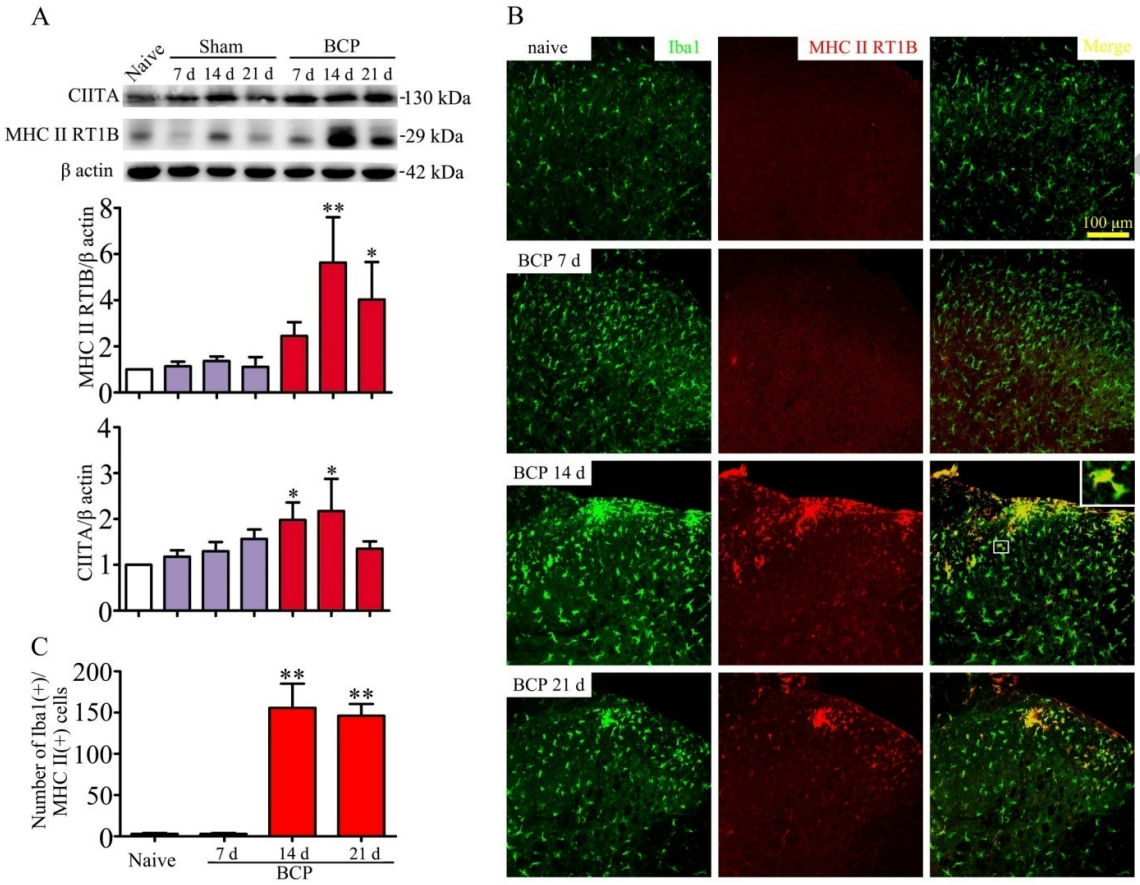

Fig. 2. CIITA and MHC II RT1B expression in the spinal cord and cell-type specificity of MHC II RT1B under BCP conditions. (A) Western blot showing the time-course of changes in CIITA and MHC II RT1B expression after BCP. Representative bands are shown as the mean±SEM. Inoculation of Walker 256 carcinoma cells induced significantly increased CIITA and MHC II RT1B expression (n=3). *P<0.05, **P<0.01 compared with the naive group. (B) Immunofluorescence showing that microglia (green, Iba1 as a biomarker) hypertrophied and proliferated following BCP induction. Double-immunofluorescence staining shows that MHC II RT1B (red) was co-expressed with Iba1 (green)-positive cells in the superficial spinal dorsal horn of BCP rats after 14 days of Walker 256 carcinoma cell inoculation (n=3). Scale bar=100 μm. (C) The number of both Iba1- and MHC II

RT1B-positive cells from lamina I to III was calculated, which was critically increased 14 days after BCP until the end of observation. **P<0.01 compared with the naive group.

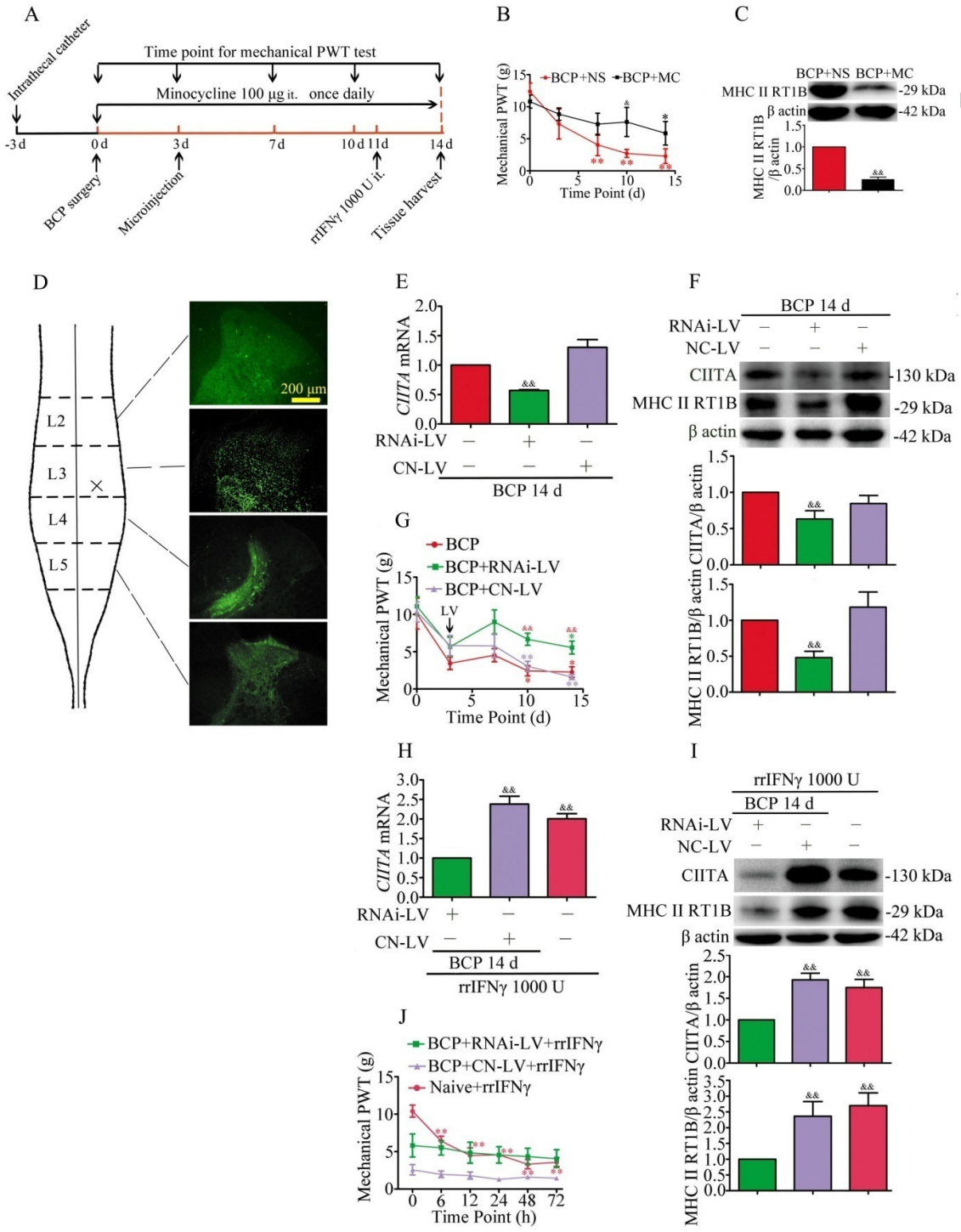

Fig. 3. MHC II mediates mechanical allodynia in BCP. (A) Schematic representing the experimental protocol. Three days prior to the establishment of the BCP model, an intrathecal

catheter operation was performed. At day 0, Walker 256 carcinoma cells were injected into the right tibial cavities of rats under pentobarbital sodium anesthesia. To assess pain perception, a mechanical paw withdrawal threshold (PWT) test was performed prior to BCP surgery (day 0) and at days 3, 7, 10 and 14 after surgery using a series of calibrated von Frey filaments. In experiment 1, minocycline (100 μg in 10 μL) or vehicle (normal saline, 10 μL) was intrathecally (it) injected once a day for 14 days. In experiment 2, lentivirus vectors (3.8×10^5 TU in 2 μL) were microinjected into the right lumbar spinal dorsal horn of BCP rats 3 days following carcinoma cell inoculation. In experiment 3, recombinant rat IFNγ (rrIFNγ, 1000 U in 10 μL) was intrathecally injected to induce the upregulation of MHC II in RNAi-LV- or CN-LV-treated BCP rats at day 11 following BCP surgery or injected into naive rats. The lumbar spinal cords (L2-L5) were collected at day 14. (B, C) The mechanical paw withdrawal threshold (PWT) was decreased from a baseline of 12.38±1.34 g to 4.05±1.68 g at day 7 and persisted to day 14 in normal saline (NS)-treated BCP rats. However, intrathecal administration of minocycline (MC) effectively ameliorated the development of mechanical allodynia and inhibited the upregulation of MHC II RT1B. (n=3). *P<0.05, **P<0.01 compared with the baseline in each group; $^{\&}P$<0.05, $^{\&\&}P$<0.01 compared between groups at each corresponding time point. (D) Single injection of lentiviral vector resulted in eGFP expression specifically in the injected dorsal horn (L3, right lateral). Scale bar=200 μm. (E) Real-time qPCR analysis revealed CIITA mRNA upregulation in BCP rats, which was attenuated by microinjection with RNAi-LV but not CN-LV (n=3 in each group). $^{\&\&}P$<0.01 compared with the BCP group. (F) Western blot analysis of CIITA and MHC II RT1B expression levels showing that both were inhibited in the BCP +RNAi-LV group but not in

the BCP + CN-LV group (n=3 in each group). $^{\&\&}P$<0.01 compared with BCP group. (G) The mechanical PWT robustly decreased in BCP and NC-LV-treated BCP rats but was preserved by RNAi-LV treatment (n=3 in each group). *P<0.05, **P<0.01 compared with the baseline in each group, $^{\&\&}P$<0.01 compared with the BCP rats at each relevant time point. (H) Intrathecal injection with recombinant rat IFNγ (rrIFNγ) increased CIITA mRNA levels in naive rats compared with RNAi-LV-treated BCP rats (n=3 in each group). $^{\&\&}P$<0.01 compared with BCP+RNAi-LV+rrIFNγ group. (I) Intrathecal rrIFNγ upregulated CIITA and MHC II RT1B protein levels in naive rats but not in RNAi-LV-treated rats (n=3). $^{\&\&}P$<0.01 compared with BCP+RNAi-LV+rrIFNγ group. (J) A single dose of rrIFNγ induced mechanical allodynia in naive rats 6 h after injection, which persisted until the end of the experiment (n=6 in each group). **P<0.01 compared with the baseline in each group.

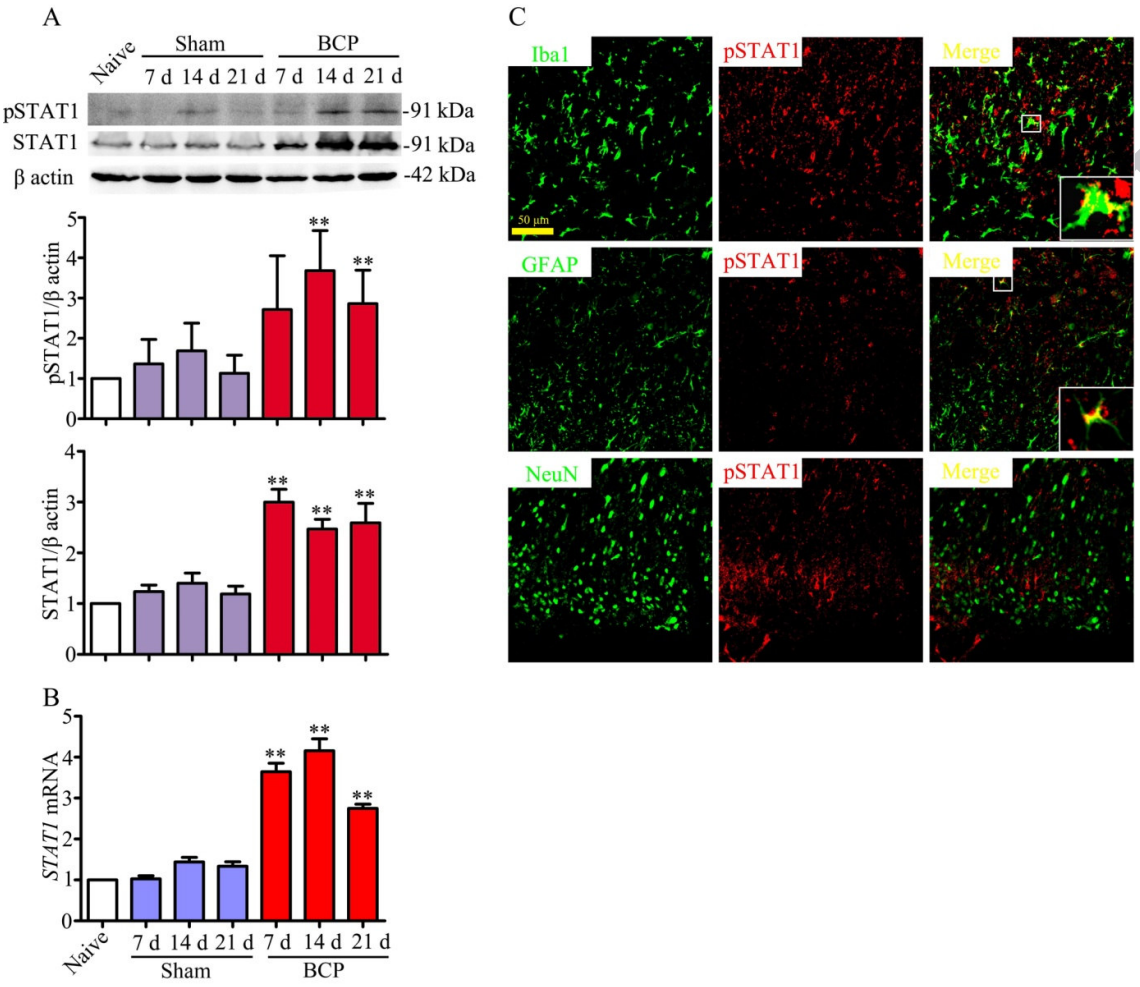

Fig. 4. pSTAT1ser727 and total STAT1 levels in the spinal cords of BCP rats and the cell-type specificity of pSTAT1ser727. (A) Western blot showing a significant difference in pSTAT1ser727 and total STAT1 in the spinal cords of BCP rats *versus* naive rats (n=3 in each group). **P<0.01 compared with the naive group. (B) STAT1 mRNA levels, as tested by real-time PCR, were consistently increased in the BCP group (n=3 in each group). **P<0.01 compared with the naive group. (C) Confocal images of pSTAT1ser727 immunostaining (red) and its colocalization with microglia (Iba1, green) or astrocytes (GFAP, green), but not with

neurons (NeuN, green) in the superficial spinal dorsal horns (lamina I to III, *n*=3 in each group). Scale bar=50 μm.

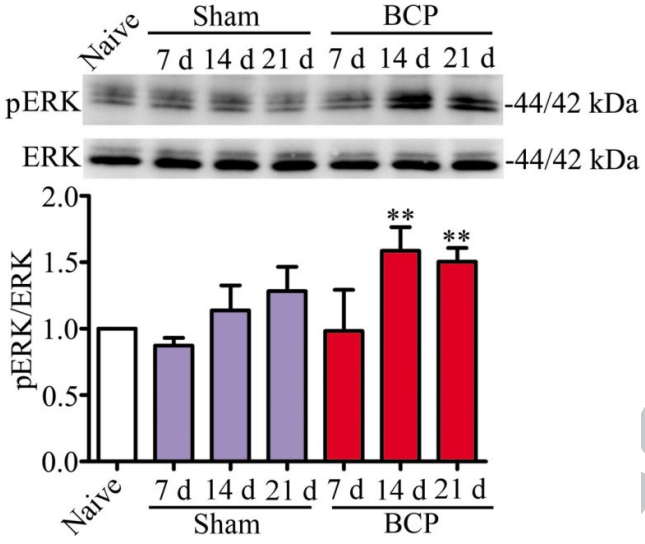

Fig. 5. ERK activation in the spinal cords of BCP rats. Western blot bands and bar graphs showing no significant difference in pERK in the sham group, compared with a significant increase in the BCP group 14 days following sarcoma inoculation, persisting until day 21 (n=3 in each group). **P<0.01 compared with the naive group.

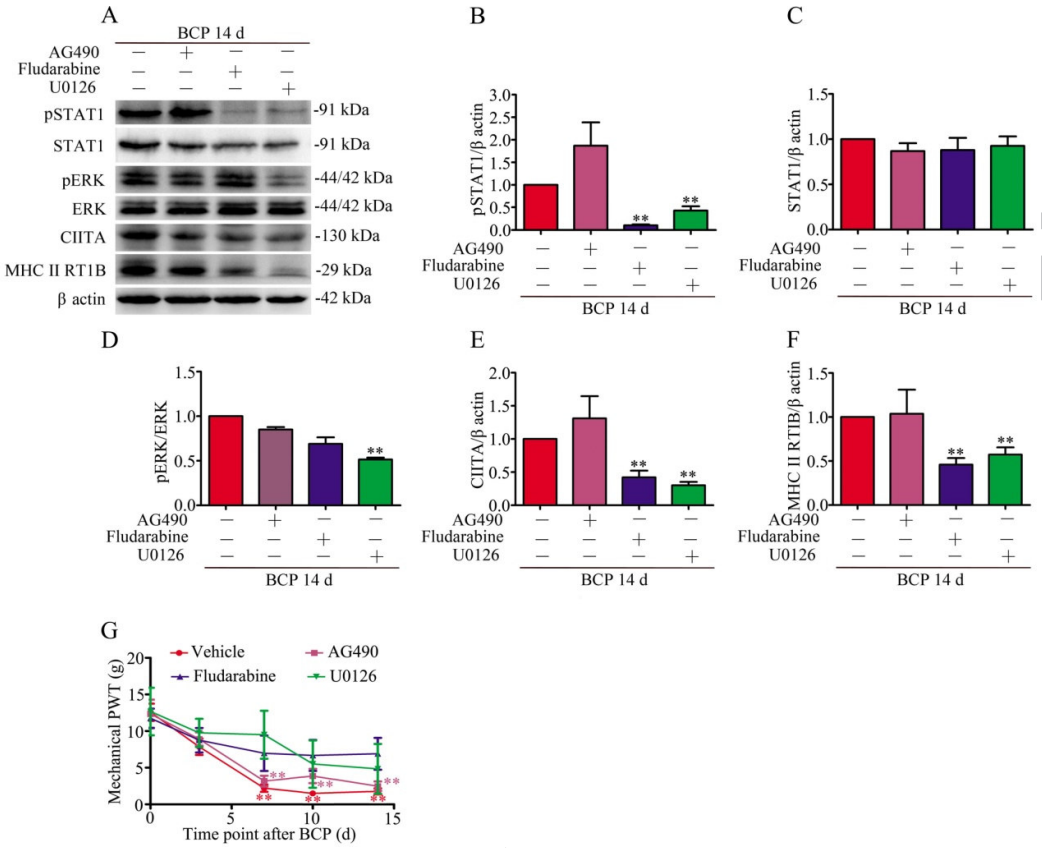

Fig. 6. ERK signaling regulates STAT1 phosphorylation, and pSTAT1 modulates MHC II expression in the spinal cord under BCP conditions. AG490 (5 μg in 10 μL), Fludarabine (10 μg in 10 μL), or U0126 (5 μg in 10 μL) was intrathecally injected into cancer-bearing rats once a day for 14 days, beginning immediately after carcinoma cell inoculation (n=3 in each group). (A) Representative western blot showing pSTAT1ser727, total STAT1, pERK42/44, total ERK42/44, CIITA, MHC II RTIB, and β actin protein levels in the spinal cords of BCP rats. (B) Bar graphs showing that Fludarabine and U0126, but not AG490, significantly inhibited the upregulation of pSTAT1ser727. (C) None of these reagents significantly altered total STAT1 levels under BCP conditions. (D) U0126, but not AG490 or Fludarabine, inhibited pERK42/44 production. (E) and (F) Both Fludarabine and U0126 blocked the increase in CIITA and MHC II RT1B expression. $^{**}P$<0.01 compared with the

normal saline-treated BCP group. In figure G, the linear graphs show that Fludarabine and U0216 effectively prevented the decrease in the mechanical paw withdrawal threshold (PWT). $^{**}P<0.01$ compared with the baseline in each group.

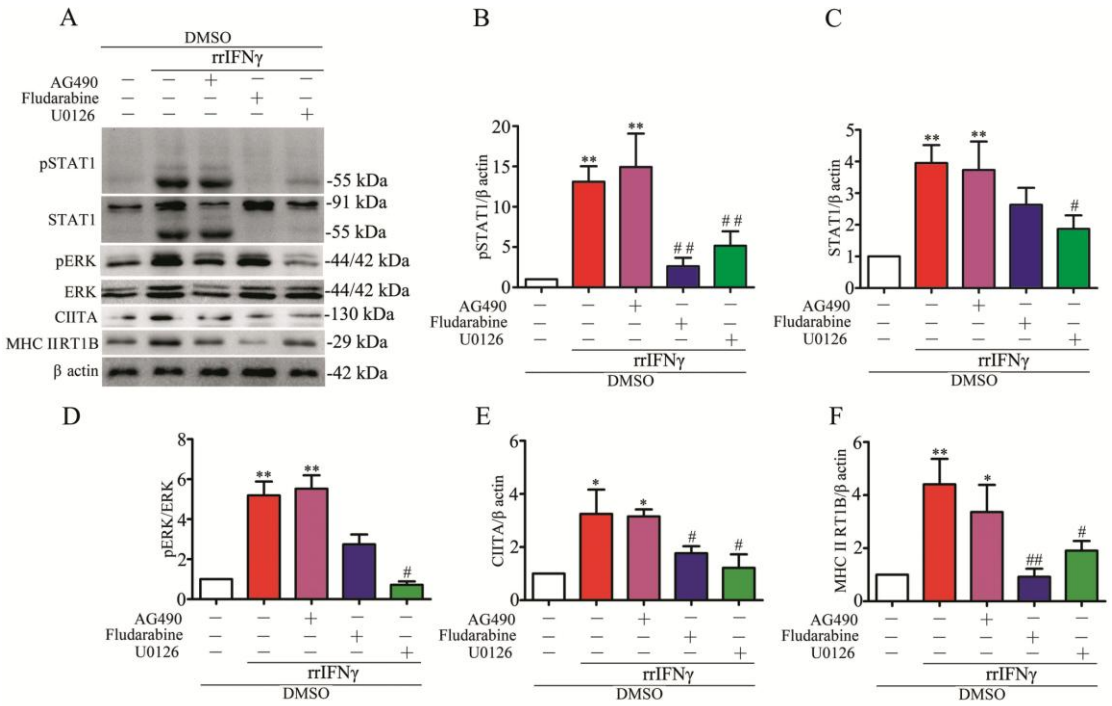

Fig. 7. ERK signaling regulates STAT1 phosphorylation to modulate MHC II expression in cultured primary microglia. Primary cerebral cortex microglia were cultured, purified, collected, and randomly divided into 5 groups (*n*=3 in each group): DMSO, recombinant rat IFNγ (rrIFNγ), AG490 +rrIFNγ, Fludarabine + rrIFNγ, and U0126 + rrIFNγ. After 24 h of stimulation, total proteins were extracted for western blot analysis. (A) Representative western blots showing pSTAT1ser727, total STAT1, pERK42/44, total ERK42/44, CIITA, MHC II RTIB, and β actin protein levels in the different groups (B, C, E, and F). pSTAT1ser727, total STAT1, CIITA, and MHC II RT1B levels were significantly increased in the rrIFNγ group and in the AG490+rrIFNγ group compared with the DMSO group but were inhibited in the Fludarabine+rrIFNγ and U0126+rrIFNγ groups compared with the rrIFNγ group. (D) Bar graph showing that pERK42/44 levels were upregulated in the rrIFNγ and AG490+rrIFNγ groups compared with the DMSO group and were selectively inhibited in the

U0126-pretreated group compared with the rrIFNγ group. **P*<0.05, ***P*<0.01 compared with the DMSO group, $^{\#}P$<0.05, $^{\#\#}P$<0.01 compared with the rrIFNγ group.

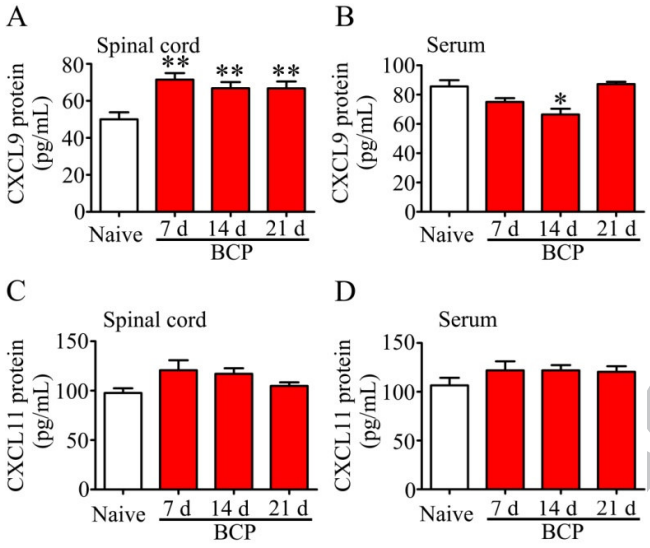

Fig. 8. CXCL9 and CXCL11 protein levels in the spinal cord and serum under BCP conditions. CXCL9 and CXCL11 protein levels were tested by ELISA. (A) The spinal level of CXCL9 was significantly increased in BCP rats. (B) However, the serum level of CXCL9 was not upregulated at any time point after BCP, and even decreased at day 14. (C, D) The change in CXCL11 levels was not statistically significant both in the spinal cord and in serum but was slightly increased compared with the naive group. **P*<0.05, ***P*<0.01 compared with the naive group.

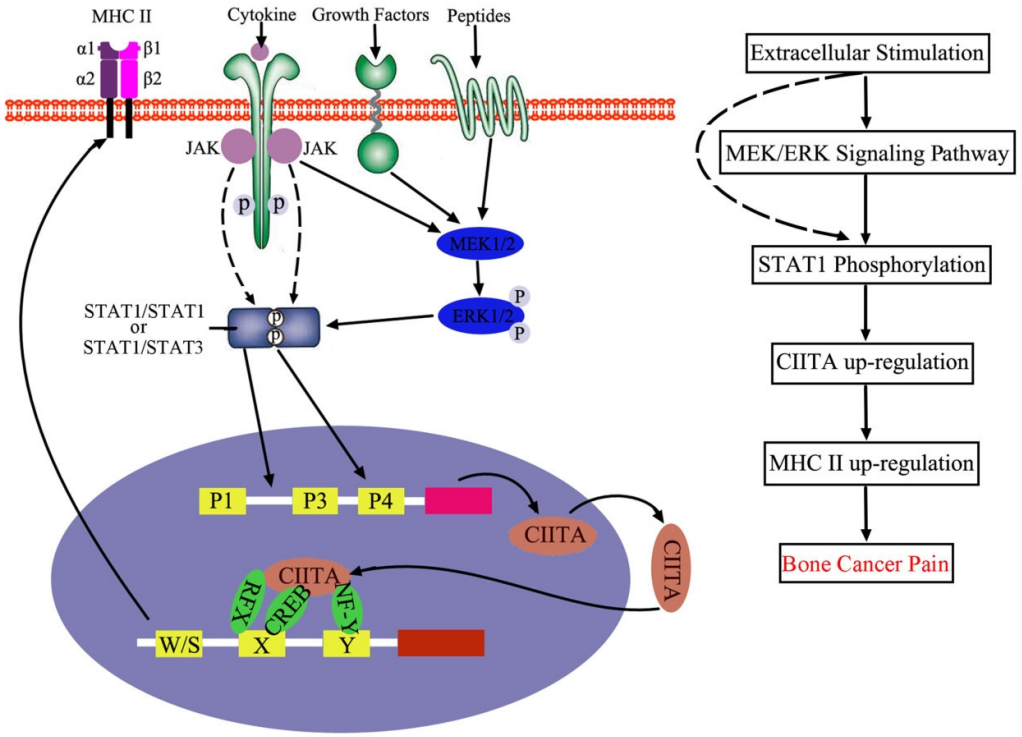

Fig. 9. A proposed model for MHC II expression in spinal microglia underlying bone cancer pain (BCP). Under BCP conditions, STAT1 acts as a downstream mediator of ERK signaling to contributes to bone cancer pain by regulating MHC II expression in spinal microglia.

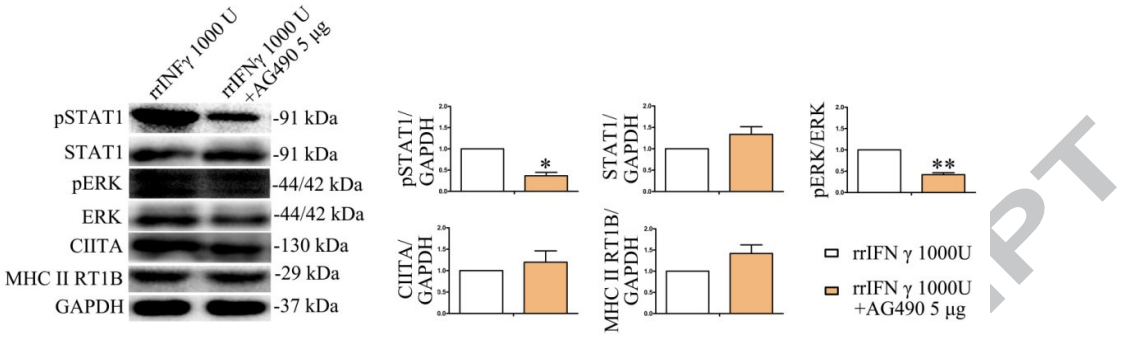

Supplemental Fig. 1. The potency of AG490 on IFNγ-induced STAT1 and ERK activation. A dose of 5 μg AG490 was intrathecally injected into naive rats 30 min prior to rrIFNγ injection (1000 U, it.); the control group was injected with the same dose of rrIFNγ. After 6 h, the enlargement of the spinal cord was collected, and protein levels were examined by western blotting. The results showed that activated pSTAT1ser727 and pERK were dramatically inhibited by 5 μg of AG490, whereas total STAT1, CIITA, and MHC II RT1B levels did not differ significantly between groups. **P*<0.05, ***P*<0.01 compared with the rrIFNγ-injected group.

- MHC II was expressed on activated microglia in the spinal cord dorsal horn of BCP rats
- STAT1 is a major mediator in modulating the expression of MHC II in microglia
- Phosphorylation of STAT1 is regulated by ERK signaling under BCP condition